

Dynamic Tensile Characterization of Vascomax[®] Maraging C250 and C300 Alloys

Bo Song¹ · Peter E. Wakeland¹ · Michael Furnish¹

Received: 15 January 2015 / Accepted: 31 March 2015 / Published online: 14 April 2015
© Society for Experimental Mechanics, Inc (outside the US) 2015

Abstract Vascomax[®] maraging C250 and C300 alloys were dynamically characterized in tension with Kolsky tension bar techniques. Compared with conventional Kolsky tension bar experiments, a pair of lock nuts was used to minimize the pseudo stress peak and a laser system was applied to directly measure the specimen displacement. Dynamic engineering stress–strain curves of the C250 and C300 alloys were obtained in tension at 1000 and 3000 s⁻¹. The dynamic yield strengths for both alloys were similar, but significantly higher than those obtained from quasi-static indentation tests. Both alloys exhibited insignificant strain-rate effect on dynamic yield strength. The C300 alloy showed approximately 10 % higher in yield strength than the C250 alloy at the same strain rates. Necking was observed in both alloys right after yield. The Bridgman correction was applied to calculate the true stress and strain at failure for both alloys. The true failure stress showed a modest strain rate effect for both alloys but no significant difference between the two alloys at the same strain rate. The C250 alloy was more ductile than the C300 alloy under dynamic loading.

Keywords Vascomax[®] maraging steel · Kolsky tension bar · Strain rate · Stress–strain · Failure

Introduction

Vascomax[®] maraging alloys are iron-based steels alloyed with 18 % nickel. The C-type maraging alloys refer to the strengthened steels with 7–12 % cobalt depending on the

grade. Such maraging steels are relatively soft in annealed condition, which makes them easily machined and formed. However, a precipitation hardening process, which requires no protective atmosphere and relatively low furnace temperatures, can significantly increase the hardness [1]. Therefore, the Vascomax[®] maraging alloys have been extensively utilized in aerospace, manufacturing, tooling, transportation, and military applications due to their superior strength. For example, they have been used for aircraft landing gears, mortar tubes, extrusion dies and drill chucks, rocket or missile motor cases, and pressure vessels. In these applications, the materials may be subjected to high-speed impact or blast loading, which requires an understanding of the dynamic behavior in terms of strength and ductility of the materials.

Kolsky tension bar techniques, which follow the same principles as the Kolsky compression bar originally developed in the 1940s [2], have been developed to characterize the dynamic stress–strain and failure responses of materials in tension [3]. Since the 1960s, a variety of Kolsky tension bar techniques have been developed to characterize the high-strain-rate tensile responses of cylindrical alloys [4–7], sheet metals [8–11], composites [12, 13], polymers [14, 15], and even biological tissues [16]. In fact, the Vascomax[®] maraging alloys have been widely used as the bar material in Kolsky bar techniques [17, 18]. However, the dynamic behavior of the Vascomax[®] maraging alloys themselves has been less characterized, particularly in tension [19]. In a general Kolsky bar experiment, in either compression or tension, pulse shaping has been required to obtain reliable resultant stress–strain response of the material under investigation [20]. The principle of the pulse shaping technique is to properly modify the profile of the incident pulse through placing a small piece of “tip” material on the impact end of the

✉ Bo Song
bsong@sandia.gov

¹ Sandia National Laboratories, Albuquerque, NM 87185, USA

incident bar. Through appropriate pulse shaping design, the stress in the specimen can be equilibrated and the strain rate held to a constant during dynamic loading; both of these are critical for obtaining reliable dynamic stress–strain response of materials. Pulse shaping can be easily applied in Kolsky compression bar tests, but can be challenging in Kolsky tension bar tests due to the different loading mechanism. A direct-tension Kolsky bar that enables easy application of the pulse shaping technique has been recently developed [18] and used to characterize a 4330-V steel in tension at high strain rates [21].

In their work, Song et al. [21] also summarized the other issues in Kolsky tension bar experiments. The first issue is to minimize the abnormal stress peak in the resultant stress–strain curve which has been observed in dynamic tensile tests on metals [6, 10, 22, 23]. This abnormal stress peak was artificial and possibly caused by the interfacial impact of the threads on the specimen and the bar ends [24]. The amplitude of the pseudo stress was reduced by applying Teflon tape on the specimen threads [24]. The threaded joint between the specimen and the bar ends also generated additional interfaces and free surfaces that modified the stress wave propagation. In this case, the reflected signal recorded by the strain gages on the incident bar represents not only the specimen response but also the threaded joint response, which consequently makes the reflected pulse no longer reliable for calculating the specimen strain and for assessing stress equilibrium in the specimen. A high-speed digital image correlation (DIC) technique was employed to check the uniformity of the specimen deformation over the entire duration of loading [21]. However, due to the limited frame rate of the high speed camera, the DIC results were not able to provide sufficient data points to construct a full stress–strain curve. Song et al. [21] attached a strain gage to the specimen surface to directly measure the specimen strain up to 2 %. When the specimen strain was over 2 %, a Micro-Epsilon[®] optoControl 1201 laser beam system was used to directly measure the displacement at the incident bar end, whereas the displacement at the transmission bar end was calculated with the transmitted signal, to calculate the total displacement applied to both gage and non-gage sections in the specimen. However, the Micro-Epsilon laser system had a relatively low resolution ($\sim 100 \mu\text{m}$) which is not adequate for small-strain measurements in the specimens with a relatively short (6.35-mm) gage length. Using high-

elongation strain gages may be another option to measure the specimen strains up to 10 % but still insufficient. An analytical correction method was proposed to calculate the actual strain in the gage section such that the tensile stress–strain curve of the material under investigation was able to be obtained [21]. However, the dynamic tensile techniques still need to be further improved for more convenient and reliable high-strain-rate stress–strain measurements in tension.

In this study, we followed the similar procedure described in Ref. [21] but further improved the specimen and experimental design as well as the specimen strain measurement in order to obtain precise and reliable dynamic engineering stress–strain curves of Vascomax[®] maraging C-250 and C-300 alloys in tension. The necking was also corrected to obtain true failure stress and strain information to compare the ductility of the two alloys.

Materials and Specimens

The materials investigated in this study are ATI Vascomax[®] maraging C250 and C300 alloys. The chemical compositions for the C250 and C300 alloys are listed in Table 1. As shown in Table 1, the C300 alloy has higher percentages of cobalt and titanium than the C250 alloy. Both the C250 and C300 alloys were normalized at 1700 F (or 927 °C) for 1 h before water quenching, and then annealed at 1500 F (or 816 °C) for 1 h before rapid air cooling. The alloys were machined into dog bone shaped cylinders with threads at both ends for dynamic tensile tests. The machined specimens were heat treated at 900 F (or 482 °C) for over 3 h and then air cooled. Figure 1 shows the geometry and dimensions of the tensile specimen. The tensile specimens were designed to have a diameter of 3.18 mm and a length of 6.35 mm in gage section. The gage section was then transitioned into 12.7-mm-diameter cylindrical ends with 1/2"-20 threads such that the tensile specimen could be directly threaded into the bar ends without the need of adapters. Ten tensile specimens were made for each material.

Hardness tests were conducted at two different locations on each end of every individual tensile specimen. The hardness test results are shown in Table 2. The C250 alloy had a mean Rockwell hardness of HRC 48.2 ± 1.3 , which corresponds to a mean yield strength of $1584 \pm 43 \text{ MPa}$. The C300 showed a higher mean Rockwell hardness of

Table 1 Chemical compositions of Vascomax[®] maraging C250 and C300 steels

	C	S	Mn	Si	Cr	Mo	Co	Ti	Al	B	Zr	Cu	P	W	Ni	Fe
C250	0.005	0.0004	0.02	0.01	0.02	4.76	7.81	0.42	0.11	0.003	<0.01	<0.01	0.003	<0.01	18.55	BAL
C300	0.004	0.0005	0.03	0.02	0.03	4.85	9.27	0.63	0.09	0.003	<0.01	<0.01	0.006	0.01	18.58	BAL

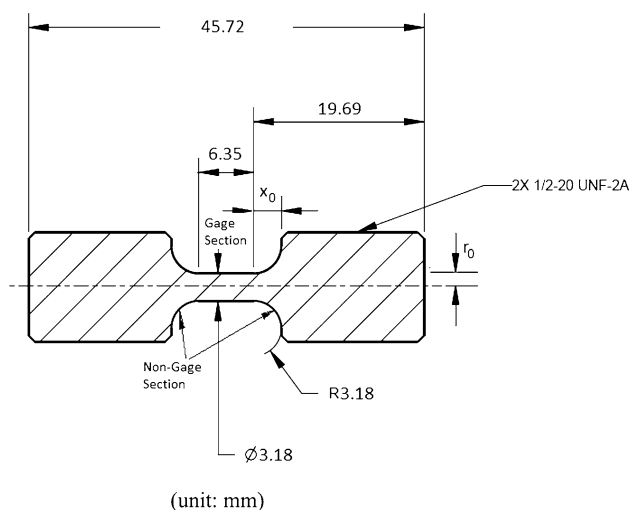


Fig. 1 Dynamic tensile specimen geometry and dimensions

HRC 51.5 ± 0.3 or mean yield strength of 1764 ± 10 MPa. The yield strength of the C300 alloy is approximately 10 % higher than that of the C250 alloy.

Dynamic Experiment

The direct-tension Kolsky bar system used in this study was the same as described in Refs [18] and [21]. The schematic of the Kolsky tension bar system is shown in Fig. 2. Both the incident and transmission bars were made of Vascomax[®] maraging C350 alloy and had a common diameter of 19.05 mm. The incident and transmission bars were 3658 and 2134 mm long, respectively. The specimen ends of both the incident and transmission bars were made into 1/2"-20 female threads such that the tensile specimen was directly threaded into the bar ends, as shown in Fig. 2. The adapters used in the previous study [21] have been removed to reduce the modification of stress wave propagation. Even though the adapters were removed in this study, the possible pseudo stress peak might still occur due to the threaded joints between the specimen and the bar ends. In order to minimize the amplitude of the pseudo peak stress, the threads between the tensile specimen and the bar ends need to be fully contacted and tightened by either directly increasing the torque or applying Teflon tape [24]. However, directly increasing

Table 2 Rockwell hardness tests of Vascomax[®] maraging C250 and C300 specimens

C250											
End	Location	2-1	2-2	2-3	2-4	2-5	2-6	2-7	2-8	2-9	2-10
1	1	52.2	47.8	50.0	49.0	48.1	48.2	48.2	48.3	51.7	48.0
	2	50.7	46.9	47.7	47.9	47.8	47.1	47.4	47.6	51.5	47.8
2	1	51.3	47.9	47.4	46.5	47.3	46.7	48.1	47.2	48.5	48.1
	2	51.1	47.1	46.9	46.4	46.6	46.4	47.7	46.4	47.9	47.9
Mean (HRC)		51.3	47.4	48.0	47.5	47.5	47.1	47.9	47.4	49.9	48.0
Yield strength (MPa)		1752	1538	1576	1546	1546	1529	1567	1538	1670	1576
C300											
End	Location	1-1	1-2	1-3	1-4	1-5	1-6	1-7	1-8	1-9	1-10
1	1	52.1	52.5	51.4	52.3	51.6	52.0	52.7	52.3	51.9	52.1
	2	51.4	51.1	51.2	50.7	51.4	50.7	50.8	51.6	51.2	50.9
2	1	51.6	52.3	51.0	51.3	51.3	51.5	52.2	52.1	51.9	52.2
	2	50.6	51.2	50.4	50.4	50.9	50.5	51.5	51.9	51.3	51.7
Mean (HRC)		51.4	51.8	51.0	51.2	51.3	51.2	51.8	52.0	51.6	51.7
Yield strength (MPa)		1758	1781	1733	1746	1752	1746	1781	1791	1769	1775

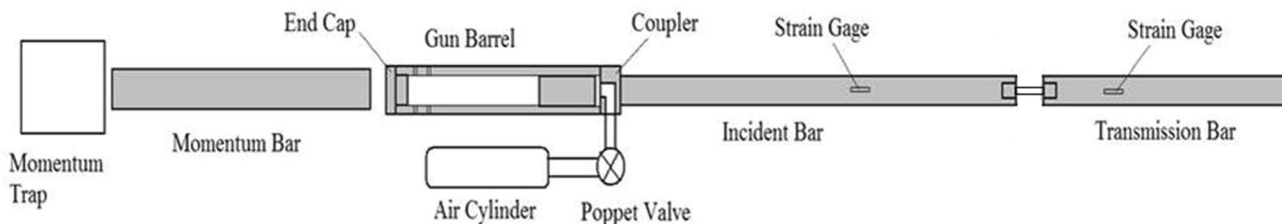


Fig. 2 Schematic of the Kolsky tension bar system

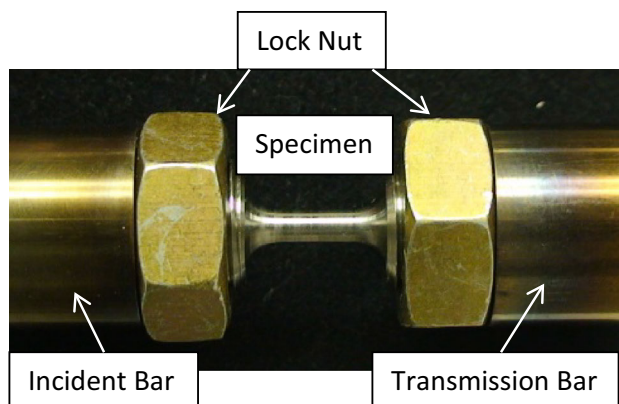


Fig. 3 Specimen assembly to the bar ends with lock nuts

the torque to the specimen during installment may generate significant shear stress in the specimen and subjects the specimen gage section to shear damage or even failure, which will consequently influence the tensile failure stress measurement. Applying Teflon tape may improve the contact of threads but the specimen can still not be sufficiently tightened for the same reason. In this study, we applied a lock nut to each end of the specimen which is shown in Fig. 3. Tightening the lock nuts produces a significant amount of tension in the threaded ends of the specimen, making a solid thread contact between the specimen and the bar ends but without generating any tension or torque to the specimen gage section. The quantitative improvement of using the lock nuts to the wave propagation and consequent measurement of the stress–strain response of the material under investigation is still in progress and will be reported later.

Though the lock nuts improved the thread contact, there existed many interfaces between the tensile specimen and the bar ends, which modified the stress wave propagation and consequently made the reflected wave no longer reliable to represent the boundary condition at the incident bar/

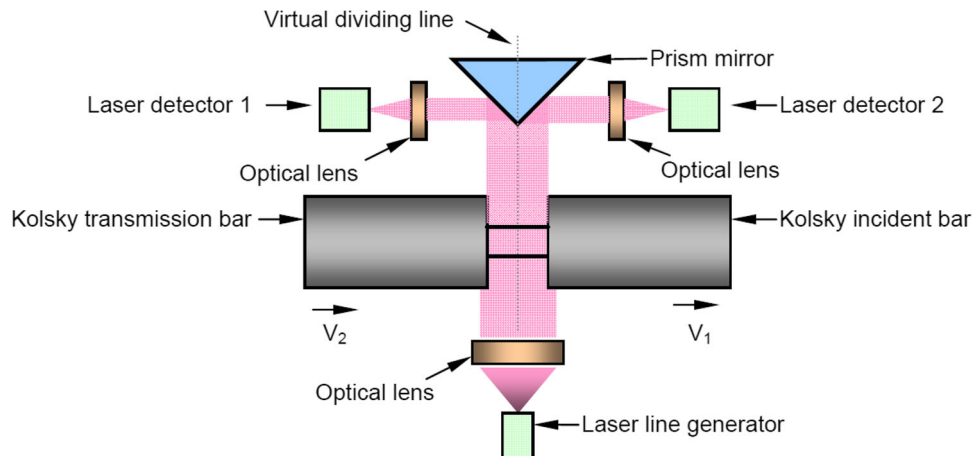
specimen interface. The unreliable reflected pulse caused difficulties in both force and displacement measurements at the incident bar/specimen interface. The digital image correlation (DIC) results in the previous study [21] showed that the stress could be equilibrated in the 6.35-mm-long gage section as long as the incident pulse was properly shaped to have a relatively long rise time. In general, it takes a longitudinal wave at least three round trips propagating through the specimen length to achieve stress equilibrium. For the material and specimen design in this study, the specimen may be equilibrated in stress within $\sim 15 \mu\text{s}$. Therefore, the rise time of the incident pulse was designed to be approximately $70 \mu\text{s}$, which is about four times longer than the time required for stress equilibrium, to ensure the stresses in the specimen equilibrated. When the specimen is in stress equilibrium, the stress in the specimen can be directly calculated with the transmitted signal, ε_t ,

$$\sigma = E_0 \frac{A_0}{A_s} \varepsilon_t \quad (1)$$

where E_0 is the Young's modulus of the transmission bar material; A_0 and A_s are cross-sectional areas of the transmission bar and the specimen at the gage section, respectively. In this study, we used the same gage length (6.35 mm) as that used in the previous study and took care to generate an incident pulse with a long rise time. It is therefore reasonable to assume that the stress in the specimen gage section is equilibrated and Eq. (1) is valid for the specimen stress calculation.

It is challenging to measure the displacement at the incident bar/specimen interface with a reasonably high resolution, particularly for small strain measurements in the specimen, even though applying a strain gage on the specimen surface is an option. In this study, we applied a new laser system to the Kolsky tension bar system. The working principle of this laser system is illustrated in Fig. 4. A

Fig. 4 Illustration of the laser displacement measurement system



uniform laser line generator was used as a light source and then split into two independent beams. The movements of the incident and transmission bars during dynamic tensile loading caused intensity changes of the laser beams that were independently detected with two separate laser detectors. Preliminary calibration and tests showed that this new laser system exhibited an excellent linearity, high frequency response and resolution [25]. More important is that the new laser system allows independently tracking the displacements at both ends of the specimen, providing more flexibility to improve the specimen strain measurement. The detail of the new laser system may be referred to Ref. [25]. The specimen strain can thus be calculated as

$$\varepsilon_m = \frac{L_1 - L_2}{L_s} \tag{2}$$

where L_1 and L_2 are displacements at incident bar/specimen and specimen/transmission bar interfaces, respectively; L_s is the gage length of the specimen. It is noted that the measurements of L_1 and L_2 include the displacements in both gage and non-gage sections. Equation (2) thus needs to be corrected in order to determine the specimen deformation in the gage section. When the specimen is in linear elasticity, the total displacements occurred on the non-gage and gage sections were calculated as [21]

$$\Delta L = 2 \int_0^{x_0} \varepsilon(x) dx = 2 \int_0^{x_0} \frac{F}{E_s \pi (R + r_0 - \sqrt{R^2 - x^2})^2} dx \tag{3}$$

$$\Delta L_s = L_s \varepsilon_s = \frac{F}{E_s \pi} \cdot \frac{L_s}{r_0^2} \tag{4}$$

where ΔL and ΔL_s are the displacements in the non-gage and gage sections, respectively, R and x_0 are respectively the radius of the transition part and the distance from the gage section to the non-gage section, r_0 is the radius of the specimen in gage section, F is the applied force, and E_s is the Young’s modulus of the specimen material. As shown in Fig. 1, $r_0 = 1.59$ mm, $R = x_0 = 3.18$ mm, and $L_s = 6.35$ mm. Equations (3) and (4) thus become

$$\Delta L = \frac{1.5368F}{E_s \pi} \text{ (mm)} \tag{5}$$

$$\Delta L_s = \frac{2.512F}{E_s \pi} \text{ (mm)} \tag{6}$$

Therefore, the elastic strain in the gage section can be corrected with a factor, c' , from the overall strain calculated with Eq. (2),

$$\varepsilon = c' \cdot \varepsilon_m = c' \cdot \frac{L_1 - L_2}{L_s} \tag{7}$$

where $c' = \frac{\Delta L_s}{\Delta L + \Delta L_s} = 0.62$.

With increasing applied force, the specimen gage section will be yielded followed by plasticity due to the smaller cross-sectional area while the non-gage section still remains in elasticity. If perfect plasticity is assumed, the displacement over the non-gage section will be a constant and can be calculated with Eq. (5)

$$\Delta L = 1.5368r_0^2 \varepsilon_y \tag{8}$$

where ε_y is yield strain. The plastic strain over the gage section can be corrected with

$$\varepsilon = \frac{L_1 - L_2 - \Delta L}{L_s} \tag{9}$$

Equations (7) and (10) provide the specimen strain measurements in elasticity and plasticity, respectively, which should be consistent at yielding,

$$\varepsilon_y = c' \cdot \frac{(L_1 - L_2)_{yield}}{L_s} = \frac{(L_1 - L_2)_{yield} - \Delta L}{L_s} \tag{10}$$

or,

$$\Delta L = (1 - c') \cdot (L_1 - L_2)_{yield} \tag{11}$$

Equation (11) indicates that, when the gage section yields, the displacement in the non-gage section can be determined with the laser displacement. The yielding in the gage section can be determined with the specimen stress history [Eq. (1)].

In a summary, after the displacements (L_1 and L_2) at both ends of the specimen are measured with the laser system, the actual strain over the specimen gage section may be calculated,

$$\varepsilon = \begin{cases} c' \cdot \frac{L_1 - L_2}{L_s} & (\sigma \leq \sigma_y) \\ \frac{L_1 - L_2 - (1 - c')(L_1 - L_2)_{yield}}{L_s} & (\sigma > \sigma_y) \end{cases} \tag{12}$$

In order to verify Eq. (12), we attached a strain gage on the specimen surface to directly measure the specimen strain up to 2 % during dynamic loading. The strain rate can be calculated with the differentiation of the specimen strain history [Eq. (12)]. After the specimen stress and strain histories are calculated, the engineering stress–strain curve of the specimen material can be obtained.

Experimental Results and Discussion

Figure 5 shows a typical set of oscilloscope records of strain gage signals on the bars and the specimen surface, as well as the laser signals, in a Kolsky tensile bar experiment on a Vascomax® C250 steel specimen (Specimen 2-1). A 610-mm-long striker was used to generate a square-like incident pulse with a rise time of ~70 μs and a total

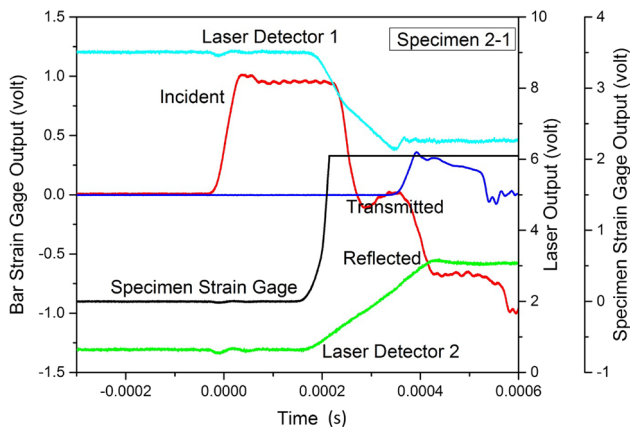


Fig. 5 A typical set of oscilloscope records of strain gage and laser measurement signals

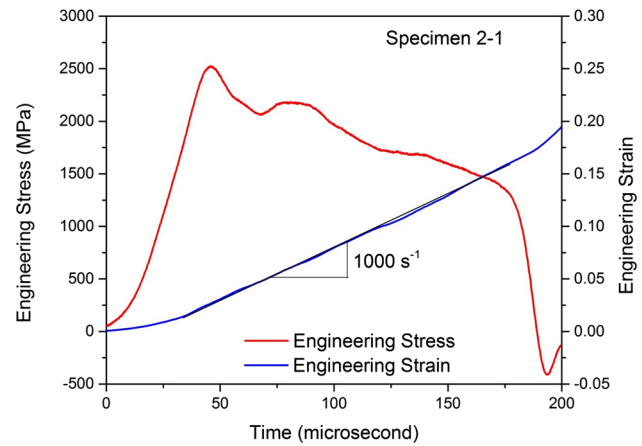


Fig. 7 Engineering stress and strain histories

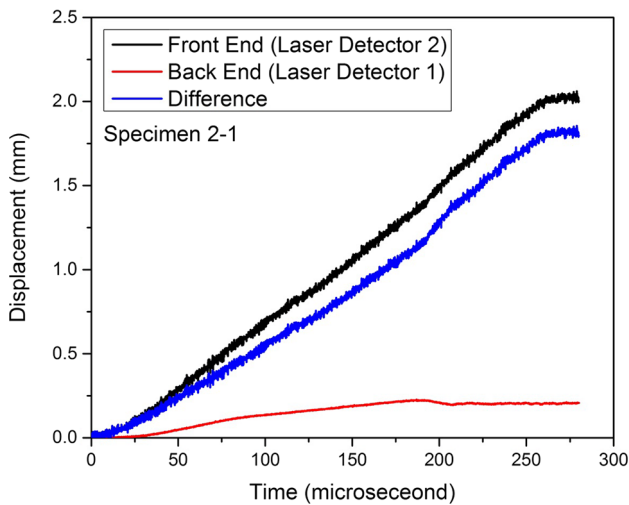


Fig. 6 Displacements at both ends of the specimen

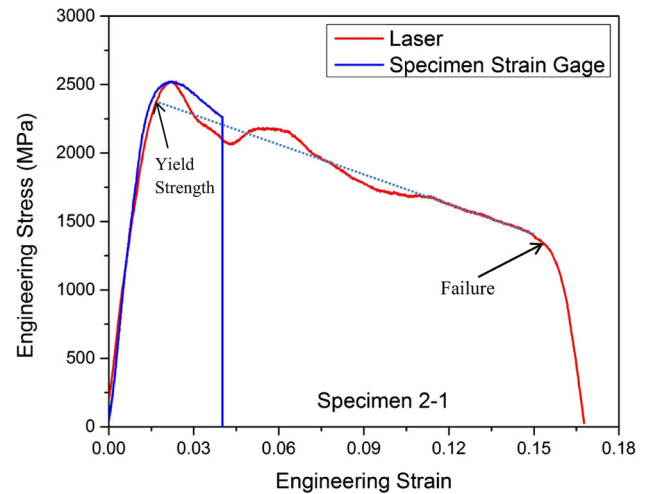


Fig. 8 Engineering tensile stress–strain curve of the Vascomax® maraging C250 steel specimen

duration of $\sim 350 \mu\text{s}$. The reflected pulse exhibits a plateau which indicates a nearly constant strain rate in the specimen under stress equilibrium. When the specimen started to fail, the strain rate suddenly increased as indicated by the sudden drop in the reflected pulse in Fig. 5. It is noted again that the reflected pulse is not reliable to be used for strain-rate calculation, due to the multiple threaded interfaces between the specimen and the bar ends. Using the lock nuts may significantly improve the contact of the threads between the specimen and the bar ends. But the quantitative effect of the lock nuts on the reflected wave and resultant stress–strain data is still under investigation. Instead, we used the laser signals shown in Fig. 5 to directly measure the specimen displacements at both ends and thence determine the specimen strain. Figure 6 shows the displacement histories at both ends of the specimen. The blue curve in Fig. 6 is the difference of the

displacements at the specimen ends, $\Delta L = L_1 - L_2$. Equation (12) was then applied to calculate the specimen strain, and the specimen stress was calculated with Eq. (1). Figure 7 shows the engineering stress and strain histories with respect to time. The strain rate was calculated from the slope of the engineering strain history, giving a nearly constant value of $\sim 1000 \text{ s}^{-1}$. The engineering stress–strain curve was therefore obtained and plotted in Fig. 8. Figure 8 also plots a stress–strain curve calculated with the direct specimen strain measurement by using the signal of the strain gage on the specimen surface. It is noted that the strain gage used on the specimen surface was able to measure the specimen strain up to 2 % in a reliable manner. The results show that the stress–strain curves from the two different measurement methods of the specimen strain are consistent, which demonstrates the reliability of the laser system measurements and the specimen strain

correction on the gage section with Eq. (12). Even though the lock nuts have been applied to minimize the pseudo stress peaks, the value of the first stress peak in the stress–strain curve may not represent the actual yield strength. In this study, we used a linear regression of the flow stress back to elastic line to estimate the yield strength, as illustrated in Fig. 6.

Following the same procedure, the Vascomax® C250 and C300 alloys were dynamically characterized in tension at two different strain rates: ~ 1000 and 3000 s^{-1} . At each condition, five experiments were repeated and the results were highly repeatable except for the specimen 2-1 due to the significantly higher hardness (Table 1). This is probably caused by the variation of the grain sizes and structures during heat treatment, which requires further microstructural investigation. A mean curve was then calculated at each strain rate and used as a representative stress–strain response at this specific strain rate. The stress–strain curve for the specimen 2-1 was not used in this calculation. Figure 9 shows the mean engineering stress–strain curves of the C250 and C300 alloys at ~ 1000 and 3000 s^{-1} . The C250 and C300 alloys exhibit very similar stress–strain characteristics which are consistent with results reported in Ref. [19]. The yield strength ($\sim 2420 \text{ MPa}$) of the C300 alloy was 11 % higher than that ($\sim 2180 \text{ MPa}$) of the C250 alloy. For the same material (C250 or C300), the tensile stress–strain responses show little difference at the strain rates of 1000 and 3000 s^{-1} . However, the dynamic yield strengths of both C250 and C300 alloys increased by 40–45 % when compared with the quasi-static hardness data shown in Table 2.

After yielding, the engineering stress decreased with increasing strain for both of the C250 and C300 steels,

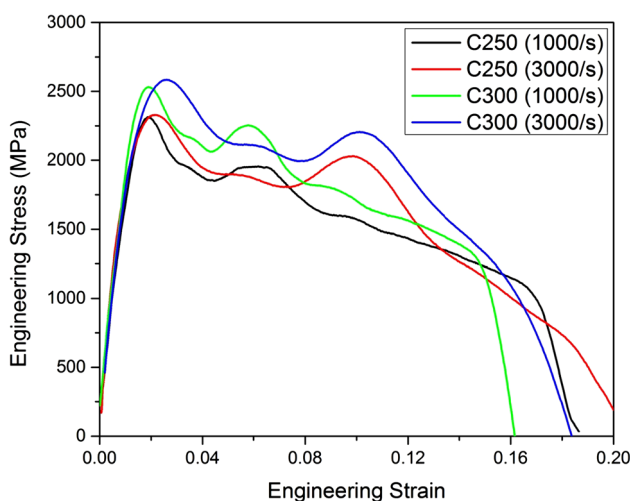


Fig. 9 Engineering tensile stress–strain curves of the Vascomax® maraging C250 and C300 steels at the strain rates of 1000 and 3000 s^{-1}

which indicates necking occurred shortly after yield. Since necking occurred very early for both of the C250 and C300 alloys, indicating significant localized deformation, the engineering stress–strain curves shown in Fig. 9 do not provide much useful information for material model development and failure analysis. Instead, the true stress–strain response needs to be determined. However, the true stress–strain response cannot be obtained until an appropriate necking correction is conducted. Here we used Bridgman correction, which requires measurements of the geometry of the observed necking [26–28], to calculate the true stress–strain response at failure.

In the Bridgman correction, the true strain and stress at the smallest cross section in the specimen when necking occurs can be calculated as [27],

$$\epsilon_T = \ln \frac{A_s}{A} \tag{13}$$

$$\sigma_T = \left[\left(1 + \frac{2R_1}{a} \right) \cdot \ln \left(1 + \frac{a}{2R_1} \right) \right]^{-1} \cdot \sigma_E \cdot \frac{A_s}{A} \tag{14}$$

where a and A are the minimum radius and cross-sectional area of the specimen at necking, respectively; and R_1 is the radius of curvature at necking. As indicated in Eqs. (13) and (14), the Bridgman correction requires instantaneous measurements of the specimen geometry and dimensions during necking, which requires the support of numerical simulation [28] or in-situ high-speed imaging on the specimen during dynamic loading. In this study, we used the geometry and dimensions of the post-mortem specimen for Bridgman correction and obtained the true stress and strain information at failure. A photograph of the same tensile specimen after dynamic testing is shown in Fig. 10. Figure 10 also illustrates the determination of the parameters,

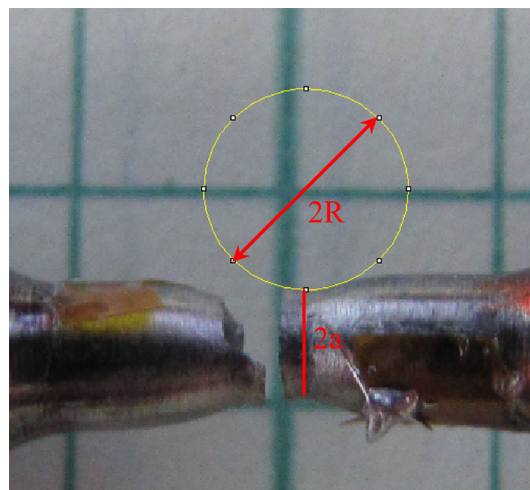


Fig. 10 Picture of the C250 tensile specimen after dynamic test (R is the radius of curvature at necking)

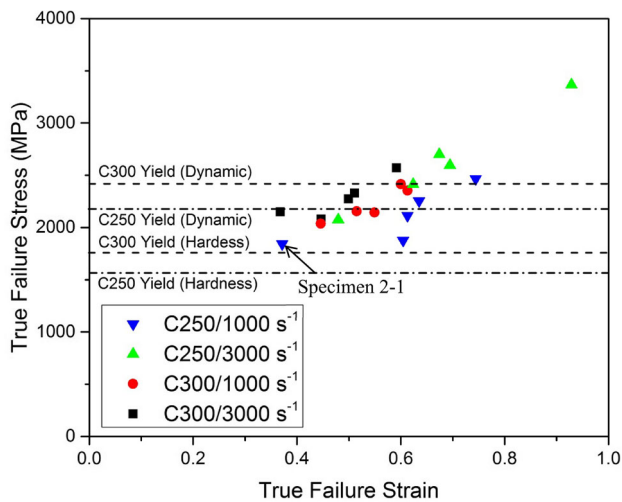


Fig. 11 True failure stresses and strains of the Vascomax[®] maraging C250 and C300 steels at the strain rates of 1000 and 3000 s⁻¹ (unit: mm)

a and R , for Bridgman correction. In this case, a and R were measured as 1.32 and 2.52 mm, respectively. The engineering stress at failure was determined from Fig. 8 as $\sigma_E = 1423$ MPa. Therefore, the true strain and stress of the specimen 2-1 at failure were calculated as $\varepsilon_{T, failure} = 0.37$ and $\sigma_{T, failure} = 1841$ MPa, respectively.

Following the same procedure, the true stress and strain yield points for all tensile specimens were determined and plotted in Fig. 11. The yield strengths for both of the C250 and C300 alloys were also indicated in Fig. 11. We also plot the mean yield strengths that were obtained from hardness tests (Table 2) for both materials in Fig. 11 for reference and comparison purposes. Again, the data for specimen 2-1 were not included in the calculation of mean yield strength for C250 alloy. Figure 11 shows the dynamic yield strengths for both C250 and C300 alloys are higher than quasi-static yield strengths obtained from hardness tests, indicating strain-rate sensitivities for both materials. The true failure stresses were very close to the dynamic yield strengths. Therefore, it is reasonable to interpret the true stress–strain response of both Vascomax[®] C250 and C300 steels to be perfectly plastic, even though the full true stress–strain curves could not be obtained after necking. The true failure strains for the C250 and C300 alloys varied from 0.35 up to 0.95, but were mostly distributed within the range of 0.45–0.7. Both the C250 and C300 alloys showed a modest strain-rate effect on the true failure stresses: the true failure stress increased by approximately 10 % when the strain rate increased from 1000 to 3000 s⁻¹. At the same strain rate, there is little difference in true failure stress between the two alloys. However, the C250 alloy exhibited larger true failure strains than the C300

alloy, meaning that the Vascomax[®] C250 alloy is more ductile than C300 alloy at high strain rates.

Conclusions

Kolsky tension bar techniques were employed to dynamically characterize the Vascomax[®] maraging C250 and C300 steels in tension at two strain rates (1000 and 3000 s⁻¹). In the Kolsky tension bar experiments, a pair of lock nuts was applied to the threaded ends of the specimen in order to minimize the pseudo peak stress in the resultant stress–strain response without applying additional tension or torque to the specimen gage section. A new laser system was applied to directly measure the displacements at both ends of the specimen with high resolution. The deformation in the specimen gage section was corrected from the measured displacement over the entire specimen length that includes both gage and non-gage sections. The C250 and C300 alloys showed little difference in the engineering tensile stress–strain response at 1000 and 3000 s⁻¹, but the dynamic yield strengths were approximately 40 % higher than those determined from quasi-static hardness tests. At the same dynamic strain rate, the C300 alloy exhibited yield and flow stresses approximately 10 % higher than did the C250 alloy. The Bridgman correction was applied to the engineering measurements to estimate the true stress and strain information at failure for both materials. The true failure stresses for the C250 and C300 alloys were approximately equal, but increased by 10 % when the strain rate increased from 1000 to 3000 s⁻¹. The C250 alloy exhibited more ductile behavior than did the C300 alloy at high strain rates.

Acknowledgments Sandia National Laboratories is a multi-program laboratory managed and operated by Sandia Corporation, a wholly owned subsidiary of Lockheed Martin Corporation, for the U.S. Department of Energy’s National Nuclear Security Administration under contract DE-AC04-94AL85000.

References

1. www.atimetals.com
2. Kolsky H (1949) An investigation of the mechanical properties of materials at very high rates of loading. Proc Phys Soc Lond B62:676–700
3. Harding J, Wood EO, Campbell JD (1960) Tensile testing of materials at impact rates of strain. J Mech Eng Sci 2:88–96
4. Nicholas T (1981) Tensile testing of materials at high rates of strain. Exp Mech 21:177–188
5. Rajendran AM, Bless SJ (1986) Determination of tensile flow stress beyond necking at very high strain rate. Exp Mech 26:319–323
6. Børvik T, Hopperstad OS, Dey S, Pizzinato EV, Langseth M, Albertini C (2005) Strength and ductility of Weldox 460E steel at

- high strain rates, elevated temperatures and various stress triaxialities. *Eng Fract Mech* 72:1071–1087
7. Arthington MR, Siviour CR, Petrinic N (2012) Improved materials characterisation through the application of geometry reconstruction to quasi-static and high-strain-rate tension tests. *Int J Impact Eng* 46:86–96
 8. Curtze S, Kuokkala V-T, Hokka M, Peura P (2009) Deformation behavior of TRIP and DP steels in tension at different temperatures over a wide range of strain rates. *Mater Sci Eng A507*:124–131
 9. Gilat A, Schmidt TE, Walker AL (2009) Full field strain measurement in compression and tensile split Hopkinson bar experiments. *Exp Mech* 49:291–302
 10. Rusinek A, Klepaczko JR (2003) Impact tension of sheet metals – effect of initial specimen length. *J Phys IV France* 110:329–334
 11. Kuroda M, Uenishi A, Yoshida H, Igarashi A (2006) Ductility of interstitial-free steel under high strain rate tension: experiments and macroscopic modeling with a physically-based consideration. *Int J Solids Struct* 43:4465–4483
 12. Lee D, Tippur HV, Jensen BJ, Bogert PB (2011) Tensile and fracture characterization of PETI-5 and IM7/PETI-5 graphite/epoxy composites under quasi-static and dynamic loading conditions. *Trans ASME J Eng Mater Technol* 133:021015
 13. Owens AT, Tippur HV (2009) Tensile stress-strain response of glass-filled epoxy under elevated rates of loading using a split Hopkinson bar apparatus. *Exp Mech* 49:799–811
 14. Brown EN, Rae PJ, Gray GT (2006) The influence of temperature and strain rate on the tensile and compression constitutive response of four fluoropolymers. *J Phys IV* 134:935–940
 15. Nie X, Song B, Ge Y, Chen W, Weerasooriya T (2009) A split Hopkinson tension bar for extra-soft specimens. *Exp Mech* 49:451–458
 16. Nie X, Cheng J-I, Chen WW (2011) Dynamic tensile response of porcine muscle. *Trans ASME J Appl Mech* 78:021009
 17. Song B, Connelly K, Korellis J, Lu W-Y, Antoun BR (2009) Improved Kolsky-bar design for mechanical characterization of materials at high strain rates. *Meas Sci Tech* 20:115701
 18. Song B, Antoun BR, Connelly K, Korellis J, Lu W-Y (2011) Improved Kolsky tension bar for high-rate tensile characterization of materials. *Meas Sci Tech* 22:045704
 19. Cinnamon JD, Palazotto AN, Brar NS, Kennan Z, Bajaj D (2006) Johnson-Cook strength model constants for VascoMax 300 and 1080 steels. In: *Shock compression of condensed matter—2005*, AIP conference proceedings, vol 845, pp 709–712
 20. Chen W, Song B (2011) *Split Hopkinson (Kolsky) bar: design, testing and applications*. Springer, New York
 21. Song B, Antoun BR, Jin H (2013) Dynamic tensile characterization of a 4330-V steel with Kolsky bar techniques. *Exp Mech* 53:1519–1529
 22. Rusinek A, Zaera R, Klepaczko JR, Cheriguene R (2005) Analysis of inertia and scale effects on dynamic neck formation during tension of sheet steel. *Acta Mater* 53:5387–5400
 23. Kuroda M, Uenishi A, Yoshida H, Igarashi A (2006) Ductility of interstitial-free steel under high strain rate tension: experiments and macroscopic modeling with a physically-based consideration. *Int J Solids Struct* 43:4465–4483
 24. Song B, Antoun BR (2012) Pseudo stress response in Kolsky tension bar experiments. *Exp Mech* 52:525–528
 25. Nie X, Song B, Loeffler CM (2015) A novel splitting-beam laser extensometer technique for Kolsky tension bar experiments. *J Dyn Behav Mater* 1:70–74
 26. Choung JM, Cho SR (2008) Study on the true stress correction from tensile tests. *J Mech Sci Tech* 22:1039–1051
 27. Ling Y (1996) Uniaxial true stress-strain after necking. *AMP J Tech* 5:37–48
 28. Mirone G (2014) The dynamic effect of necking in Hopkinson bar tension tests. *Mech Mater* 58:84–96